Loss of Erk3 function in mice leads to intrauterine growth restriction, pulmonary immaturity, and neonatal lethality

Sonia Klinger[a,1], Benjamin Turgeon[a,b,1], Kim Lévesque[a], Geoffrey A. Wood[c], Kjersti M. Aagaard-Tillery[d,e], and Sylvain Meloche[a,b,f,2]

[a]Institut de Recherche en Immunologie et Cancérologie and Departments of [f]Pharmacology and [b]Molecular Biology, Université de Montréal, Montreal, QC, Canada H3C 3J7; [c]Department of Pathobiology, Ontario Veterinary College, University of Guelph, Guelph, ON, Canada N1G 2W1; [d]Department of Pediatrics, Division of Neonatology, University of Utah Health Sciences, Salt Lake City, UT 84112; and [e]Department of Obstetrics and Gynecology, Division of Maternal-Fetal Medicine, Baylor College of Medicine, Houston, TX 77030

Edited by Melanie H. Cobb, University of Texas Southwestern Medical Center, Dallas, TX, and approved August 10, 2009 (received for review January 28, 2009)

Extracellular signal-regulated kinase 3 (Erk3) is an atypical member of the mitogen-activated protein (MAP) kinase family. No function has yet been ascribed to this MAP kinase. Here we show that targeted disruption of the *Mapk6* gene (encoding Erk3) leads to intrauterine growth restriction, associated with marked pulmonary hypoplasia, and early neonatal death during the first day of life. Around 40% of Erk3$^{-/-}$ neonates die within minutes after birth from acute respiratory failure. Erk3-deficient mice have normal lung-branching morphogenesis, but show delayed lung maturation characterized by decreased sacculation, atelectasis, and defective type II pneumocyte differentiation. Interestingly, in utero administration of glucocorticoid promoted fetal lung maturity and rescued differentiation of type II cells, but failed to alter the neonatal lethality. We observed that loss of Erk3 retards intrauterine growth, as reflected by a marked reduction in fetal lung, heart, and liver weights, and by low body weight at birth. Importantly, we found that insulin-like growth factor (IGF)-2 levels are decreased in the serum of Erk3-deficient mice. Our findings reveal a critical role for Erk3 in the establishment of fetal growth potential and pulmonary function in the mouse.

gene targeting | MAP kinase | lung | IUGR

MAP kinases are a family of serine/threonine kinases that play a key role in transducing environmental stimuli into a wide range of intracellular responses (1). In mammals, 14 MAP kinase genes have been identified that define seven distinct MAP kinase signaling pathways (2). The classical MAP kinases are phosphorylated and activated by members of the MAP kinase kinase/Mek family and comprise the well-characterized Erk1/Erk2, Jnk1/2/3, p38$\alpha/\beta/\gamma/\delta$, and Erk5 enzymes. Atypical MAP kinases include Erk3/Erk4, NLK, and Erk7. Much less is known about the mechanisms of regulation, substrate specificity, and physiological functions of this latter group of MAP kinases.

The Erk3 gene was originally identified by homology-based cloning using the Erk1 cDNA as probe (3). Erk3 exists as a 100-kDa protein consisting of a kinase domain at the N terminus followed by a unique C-terminal extension of unknown function (3–5). Despite the significant homology of their kinase domains, several properties distinguish Erk3 from Erk1/Erk2 and other classical MAP kinases. Erk3 contains a single phospho-acceptor site in the activation loop instead of the canonical dual phosphorylation motif Thr-Xaa-Tyr. Unlike classical MAP kinases, activation loop phosphorylation of Erk3 is detected in resting cells and is minimally modulated by mitogenic or stress stimuli (6). Functionally, Erk3 does not phosphorylate generic MAP kinase substrates such as myelin basic protein [(7); unpublished data], indicating that it has different or more restricted substrate specificity. The only substrate of Erk3 that has been identified so far is the MAP kinase-activated protein kinase MK5 (8, 9).

Structurally, Erk3 is most closely related to the MAP kinase Erk4. The two proteins display 73% amino acid identity in the kinase domain and share the same Ser-Glu-Gly sequence in their activation loop. Furthermore, the structural organization of the Erk3 gene (*Mapk6*) is similar to that of the Erk4 gene (*Mapk4*), suggesting that the two genes arose by duplication of a common ancestor (10). Of note, the Erk3 and Erk4 genes are the only MAP kinase genes whose expression is restricted to vertebrates, implying a role in more specialized vertebrate-specific physiological processes.

The physiological function of Erk3 remains to be elucidated. The expression of Erk3 is temporally regulated during embryonic development, increasing at the time of early organogenesis and then declining gradually toward birth (3, 11, 12). In adult animals, Erk3 mRNA is detected in most tissues, with the highest levels found in the central nervous system and skeletal muscle (3, 12). In vitro studies have shown that Erk3 expression is up-regulated during terminal differentiation of model cell lines into neurons or myotubes (3, 13). Prolactin treatment also increases Erk3 expression in isolated rat pancreatic islets (14). Altogether, these studies suggest a putative role for Erk3 in regulating cellular differentiation. To characterize the function of Erk3 in vivo, we generated Erk3-deficient mice by targeted replacement of the *Mapk6* coding region with the *LacZ* reporter gene. We show that loss of Erk3 leads to respiratory distress and early neonatal lethality, associated with intrauterine growth restriction (IUGR), pulmonary hypoplasia and impairment of type II pneumocyte differentiation. Of clinical interest, in utero administration of glucocorticoids promoted fetal lung maturity and rescued pneumocyte differentiation but did not alter the neonatal course. Our findings identify a critical role for Erk3 in fetal growth and lung maturation.

Results

Generation of Erk3-Deficient Mice. To inactivate the *Mapk6* gene, we inserted a *LacZ* reporter gene in frame with the ATG initiation codon located in exon 2 of *Mapk6* (10), resulting in deletion of the sequences encoded by exons 2, 3, and 4. The *LacZ* gene provides a stop codon and a polyadenylation signal

Author contributions: S.K., B.T., and S.M. designed research; S.K., B.T., K.L., G.A.W., and K.M.A.-T. performed research; S.K., B.T., G.A.W., K.M.A.-T., and S.M. analyzed data; and S.K., B.T., K.M.A.-T., and S.M. wrote the paper.

The authors declare no conflict of interest.

This article is a PNAS Direct Submission.

[1]S.K. and B.T. contributed equally to this work.

[2]To whom correspondence should be addressed. E-mail: sylvain.meloche@umontreal.ca.

This article contains supporting information online at www.pnas.org/cgi/content/full/0900919106/DCSupplemental.

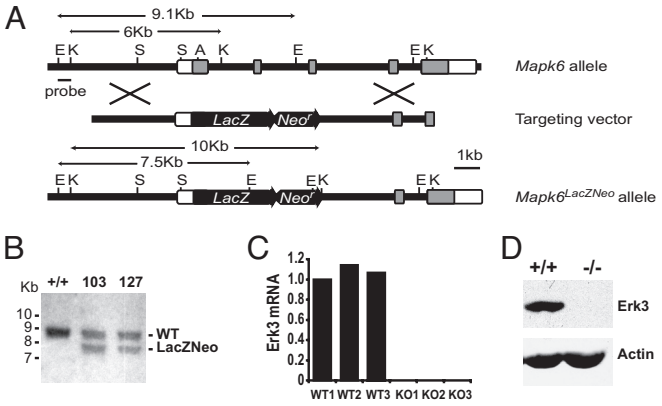

Fig. 1. Targeted disruption of the *Mapk6* gene. (*A*) Schematic representation of the *Mapk6* locus, targeting vector and recombinant allele. The targeting vector carries a neomycin resistance gene (*Neo*^{r}) and the *LacZ* gene fused in frame with the *Mapk6* coding sequence 12 amino acids downstream of the initiation codon. Exons 2 to 6 and restriction sites are shown (E, *Eco*R1; K, *Kpn*I; S, *Spe*I; A, *Apa*I). Open boxes correspond to UTRs and dark boxes indicate coding regions. Introns are shown as bars. (*B*) Southern blot analysis of *Eco*RI-digested genomic DNA from two correctly targeted ES clones indicating the wild-type (9.1 kb) and mutant (7.5 kb) alleles. (*C*) Quantitative RT-PCR analysis of Erk3 mRNA isolated from the lungs of wild-type and *Mapk6* null embryos at E18.5. Results are expressed relative to WT1. (*D*) Immunoblot analysis of Erk3 protein expression in cellular extracts prepared from wild type and *Mapk6*$^{-/-}$ mouse embryonic fibroblasts.

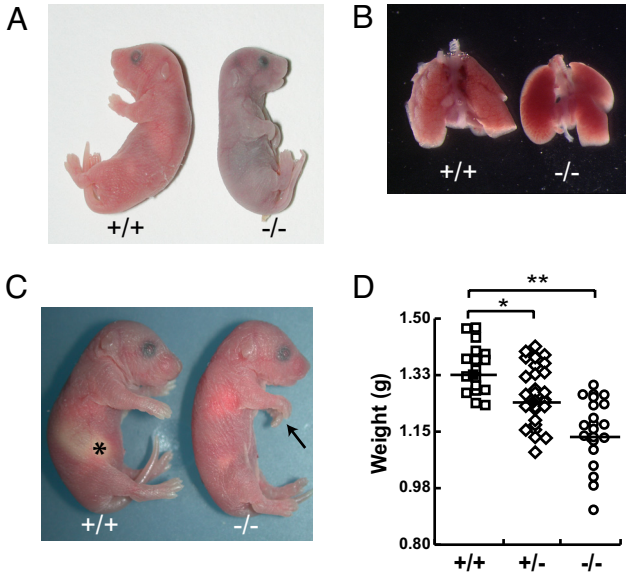

Fig. 2. Deletion of *Mapk6* leads to neonatal lethality. (*A*) Representative photograph of a cyanotic Erk3$^{-/-}$ pup and wild-type littermate immediately after birth. (*B*) Lungs isolated from a wild-type newborn are well inflated as compared to those of a dead Erk3$^{-/-}$ mouse. (*C*) Erk3$^{-/-}$ newborns surviving acute respiratory failure lack milk (*) in their stomach. Note the carpoptosis (arrow) in the Erk3$^{-/-}$ mouse. (*D*) Body weight distribution of Erk3$^{+/+}$, Erk3$^{+/-}$, and Erk3$^{-/-}$ newborns after birth. The mean body weight is indicated for each genotype: Erk3$^{+/+}$, 1.34 ± 0.07 g (n = 18); Erk3$^{+/-}$, 1.27 ± 0.09 g (n = 31); Erk3$^{-/-}$, 1.18 ± 0.08 g (n = 21). *, $P < 0.05$; **, $P < 0.01$.

and is predicted to generate a null allele (Fig. 1*A*). Chimeric mice were derived from two independently targeted R1 embryonic stem (ES) cell clones, which both transmitted the mutant *Mapk6* allele to the germ line as determined by Southern blot analysis (Fig. 1*B*). The same phenotype was observed in mutant animals generated from the two clones. To confirm that the targeted *Mapk6* allele was null, the expression of Erk3 was analyzed in tissues isolated from litters of heterozygous intercrosses. Quantitative RT-PCR analysis of E18.5 embryonic lung RNA documented the complete absence of Erk3 transcript in homozygous *Mapk6* mutants (Fig. 1*C*). Accordingly, no Erk3 protein was detected in cell extracts from embryonic fibroblasts isolated from these mutants (Fig. 1*D*).

The insertion of *LacZ* at the locus of *Mapk6* allowed us to examine the pattern of Erk3 gene expression during mouse development. Histochemical staining of β-galactosidase activity in E15.5 embryos showed that Erk3 is differentially expressed in a wide range of developing tissues (Fig. S1 and Table S1).

Loss of Erk3 Leads to Neonatal Death. Genotype analysis of litters from *Mapk6*$^{+/-}$ intercrosses failed to identify any homozygous mutant offspring at weaning. Careful analysis of timed pregnancies revealed that Erk3$^{-/-}$ mice are born with normal Mendelian frequency, but that no homozygous mutant can be found between postnatal days 2–5, indicating that loss of Erk3 results in neonatal lethality within a 24-h interval after birth (Table S2). To determine the precise onset of mortality and get insight into the underlying cause of death, we closely monitored the fate of newborn mice during delivery and in the following hours. Around 40% (12/31 mice) of Erk3$^{-/-}$ neonates showed severe respiratory distress and died within 15 min of delivery. These mutant mice made visible efforts to breathe, but remained cyanotic and died of acute respiratory failure (Fig. 2*A*). The lungs dissected from compromised neonates were not inflated with air (Fig. 2*B*) and sank with saline immersion (data not shown). Histological analysis of serial sections of Erk3$^{-/-}$ embryos and neonates by two independent pathologists did not reveal any gross morphological anomaly of internal organs (data not shown) or structural defect in the diaphragm and intercostal muscles (Fig. S2). Importantly, the heart did not exhibit any morphological abnormality (Fig. S3). Moreover, no skeletal defect was observed in the thorax of Erk3 mutants (Fig. S4). The approximately 60% (19/31 mice) of Erk3$^{-/-}$ newborns that survived the immediate neonatal interval displayed uncoordinated movements, lack of reflex on pinching, infirm vocalization, and diminished suckling reflex compared to wild-type littermates. The inability to suckle was confirmed by the absence of milk in the stomach on necropsy (Fig. 2*C*). This second group of mutant animals subsequently died within 24 h of delivery, and is not the subject of further characterization in this report.

Regardless of the interval of neonatal demise, Erk3$^{-/-}$ mice exhibited kyphosis and carpoptosis, and diminished fetal growth (Fig. 2 *C* and *D* and Fig. S4). At birth, the body weight of Erk3 null mutants was reduced by 10–15% as compared to wild-type littermates: Erk3$^{+/+}$, 1.34 ± 0.07 g versus Erk3$^{-/-}$, 1.18 ± 0.08 g, $P < 0.01$ (Fig. 2*D*). Notably, Erk3$^{+/-}$ heterozygous mice were also significantly lighter than wild type mice (1.27 ± 0.09 g, $P < 0.05$), indicating that the loss of a single allele of *Mapk6* is sufficient to restrict fetal growth.

Histological Analysis of Erk3-Deficient Lungs. Given the well-recognized contribution of diminished functional respiratory capacity to neonatal mortality, we sought to closely inspect the architecture and histology of the lungs in *Mapk6* null mice. Overall organogenesis of the lungs was preserved in mutant mice with four right lobes and a single left lobe flanking the heart (Fig. 2*B*). Blinded evaluation of hematoxylin/eosin-stained lung sections at E12.5, E14.5, and E16.5 failed to reveal any observable difference in branching morphogenesis between Erk3$^{-/-}$ mice and wild-type littermates (Fig. 3*A*). However, at E18.5, both subjective observation (Fig. 3*A*) and quantitative morphometric measurement (Fig. 3*B*) demon-

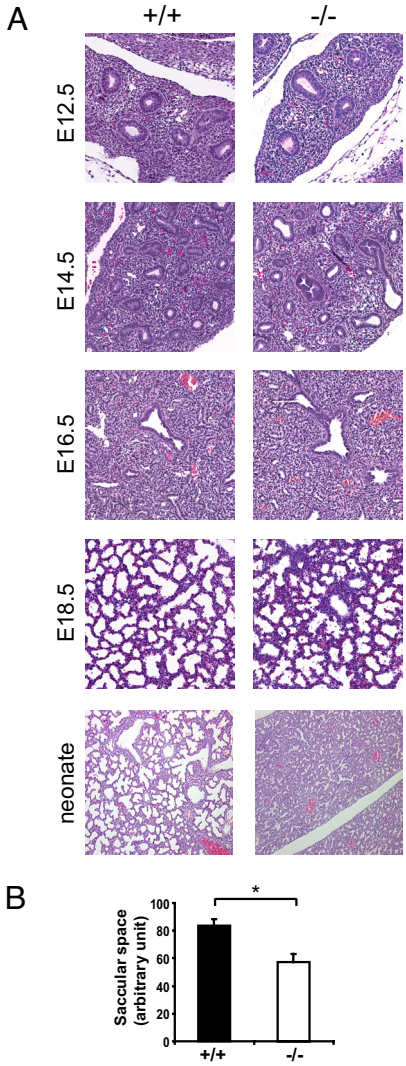

Fig. 3. Histological analysis of the developing lung in wild-type and Erk3$^{-/-}$ mice. (*A*) Lung sections from littermate Erk3$^{+/+}$ and Erk3$^{-/-}$ embryos were prepared at the indicated developmental stages and stained with hematoxylin and eosin. Magnification, 20×. (*B*) Morphometric analysis of lung saccular airspace in E18.5 wild-type and Erk3$^{-/-}$ embryos (n = 5–6). *, $P < 0.01$.

strated diminished saccular space with concomitant increased mesenchymal tissue in the lungs of Erk3$^{-/-}$ embryos (32% decrease, $P < 0.01$). As anticipated, the lungs of Erk3 mutant neonates found in distress displayed extensive and severe atelectasis (Fig. 3*A*). The observation of normal branching morphogenesis with impaired saccular development is suggestive of a lung maturation defect in Erk3-deficient mice.

Loss of Erk3 Results in Abnormal Maturation of Distal Lung Epithelium. In light of the above findings, we next sought to determine whether Erk3$^{-/-}$ lungs manifest developmental defects of the saccular structures. The distal epithelium is comprised of two specialized cell populations: squamous type I pneumocytes, which are responsible for gas exchange, and cuboidal type II pneumocytes, which produce surfactant for maintenance of alveolar surface tension. We first tested the distensibility of the lungs by instilling fixative into the trachea of E18.5 embryos. There was no major difference in the histology of the lungs of control and mutant littermates, indicating that type I pneumocytes form functional respiratory saccules (Fig. 4*A*). The differentiation of type I pneumocytes was further assessed by immunohistochemistry analysis. Immunostaining for T1α (podoplanin), a membrane protein marker of type 1 cells, on E18.5 lung sections similarly failed to reveal any significant difference in T1α expression between mutant and wild type mice (Fig. 4*B*), suggesting normal cell differentiation. The differentiation of type II pneumocytes was assessed by analyzing the expression of pulmonary surfactant-associated protein (SP)-C and the content of cytoplasmic glycogen, which serves as a substrate for surfactant phospholipids (15), in lungs from E18.5 embryos. Staining of SP-C was not altered in Erk3$^{-/-}$ mice (Fig. 4*C*). However, ultrastructure analysis by electron microscopy revealed that type II pneumocytes from Erk3 mutant mice contain abundant glycogen granules and present attenuated villi when compared to controls, a symptom of pulmonary immaturity (Fig. 4*D*). To further substantiate this idea, we also measured the intracellular glycogen content by staining lung sections with periodic acid-Schiff (PAS). A major increase in the number of cells containing cytoplasmic glycogen was observed in Erk3 mutant embryos (Fig. 4 *E* and *F*). These results indicate that type II pneumocytes of Erk3$^{-/-}$ mice differentiate to the stage of being able to synthesize surfactant-associated proteins, but they cannot complete their differentiation program, as demonstrated by their inability to properly use intracellular glycogen for the synthesis of surfactant lipids.

In Utero Glucocorticoid Administration Rescues Type II Pneumocyte Differentiation but Fails to Abrogate Neonatal Lethality. Since the initial observation that dexamethasone induces inflation of fetal lungs in premature lambs, antenatal glucocorticoids have come to serve as the mainstay of clinical management of pregnancies complicated by IUGR and risk of preterm birth for the promotion of fetal lung maturity (16). To determine if the neonatal mortality of Erk3$^{-/-}$ mice was attributable to pulmonary immaturity, we asked whether transplacental administration of dexamethasone improves the neonatal outcome. Dexamethasone treatment of pregnant mice for 48 h before delivery significantly improved the immature saccular architecture of Erk3$^{-/-}$ lungs, as demonstrated by complete restoration of the saccular airspace (Fig. 5*A*) and reduction of the number of immature glycogen-containing cells to normal values (Fig. 5*B*). However, antenatal dexamethasone did not ameliorate the survival of Erk3$^{-/-}$ mice, which remained cyanotic and died in the neonatal interval.

Erk3$^{-/-}$ Mice Display Intrauterine Growth Restriction and Pulmonary Hypoplasia. Respiratory distress syndrome is a serious complication of premature and intrauterine growth-restricted infants and represents the primary contributor to neonatal morbidity and mortality (17). It affects up to 20% of low birth weight infants (classically defined as <2,500 grams) and as great as 70% of growth restricted fetuses (<10th % adjusted for gestational age). Respiratory failure in these infants presumptively occurs as a result of surfactant deficiency and pulmonary hypoplasia. Given our initial observations of fetal growth discrepancy and pulmonary immaturity in Erk3-null fetuses, we sought to establish growth velocity curves and assess the proliferation rate of lung cells in our genetic mouse model.

Erk3$^{-/-}$ embryos and wild-type littermates were collected at different gestational stages, starting at E13.5, and their body weights were compared. No significant difference was observed between mutant and control animals at early gestation, although a trend toward a decrease was already noticeable at E14.5 (Fig. 6*A*). However, from E14.5 onwards, adjusted fetal weights of Erk3$^{-/-}$ embryos were significantly reduced by 11–18% (Fig. 6*A*). To discern relative skeletal versus visceral abnormalities, we further analyzed the individual weights of

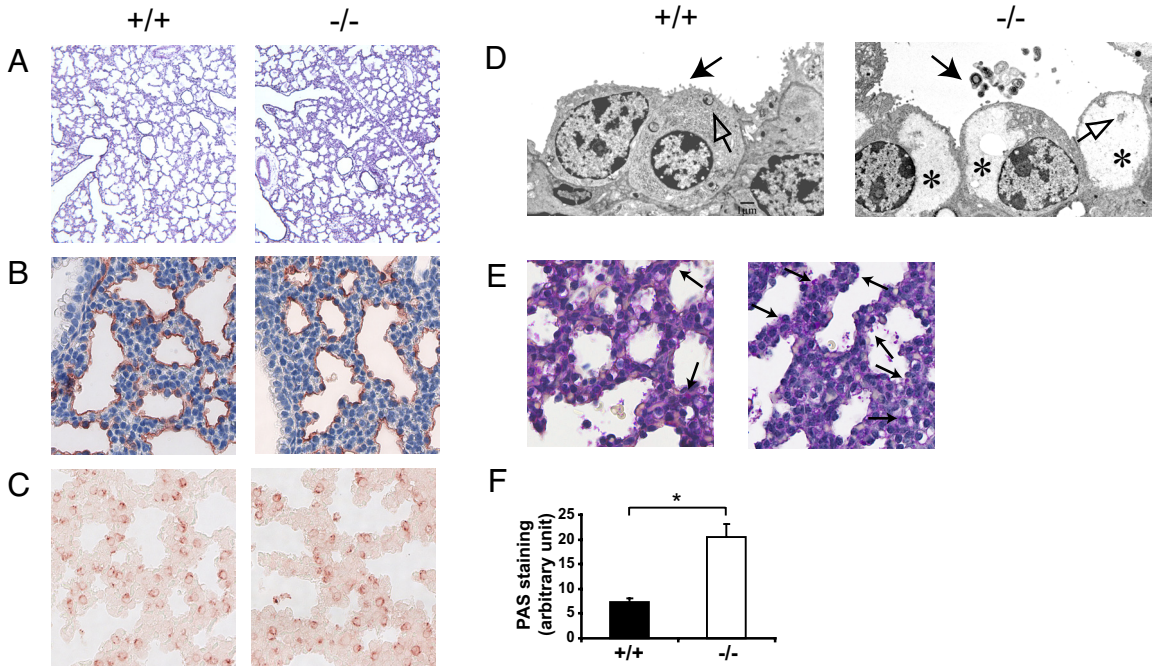

Fig. 4. Defective maturation of the distal lung epithelium in Erk3-deficient mice. (*A*) Sections of E18.5 Erk3$^{+/+}$ and Erk3$^{-/-}$ lungs inflated with fixative were stained with hematoxylin and eosin. Magnification, 5×. Immunostaining for T1α (*B*) and SP-C (*C*) in lungs from littermate wild-type and Erk3$^{-/-}$ embryos at E18.5. Magnification, 40×. (*D*) Ultrastructure of E18.5 Erk3$^{+/+}$ and Erk3$^{-/-}$ lungs. Mature type II pneumocytes present characteristic villi (black arrow) and contain lamellar bodies (open arrow). Type II cells from Erk3-deficient lungs contain an abundant pool of glycogen (*) and present attenuated villi. Secreted surfactant can be observed occasionally in the airspace of Erk3$^{-/-}$ embryos (black arrow). (*E*) PAS staining (arrows) indicating cytoplasmic glycogen in lung sections from E18.5 wild-type and Erk3$^{-/-}$ embryos. Magnification, 40×. (*F*) Quantification of PAS staining (n = 5–6). *, $P < 0.01$.

the lung, heart and liver in E18.5 embryos. We found that the absolute organ weights of Erk3$^{-/-}$ animals were reduced by 25–40% as compared to their wild type littermates (Fig. 6*B* and Fig. S5), in the absence of any apparent morphological defect. Likewise, the ratio of organ to body weight was significantly decreased in Erk3-null mutants, the lung and the heart showing the greatest reduction (Fig. 6*C*).

To further characterize the pulmonary hypoplasia phenotype of Erk3 mutant mice, we analyzed the proliferation rate of lung cells by Ki67 immunostaining. At E18.5, the number of proliferating cells in Erk3$^{-/-}$ lungs was reduced by 60% as compared to wild-type lungs (Fig. 6*D*). Analysis of cell proliferation throughout lung development showed that the decrease in Ki67-positive cells is already apparent at E12.5 and reaches significance at E16.5 (Fig. 6*D*). Thus, loss of Erk3 results in impairment of lung cell proliferation from the early stages of pulmonary development, in parallel to restriction of fetal growth.

Earlier studies have demonstrated the importance of the IGF signaling axis for embryonic and postnatal body growth (18, 19). To elucidate the molecular basis of the IUGR phenotype, we measured the fetal levels of IGF-1 and IGF-2. We found similar IGF-1 levels in the serum of Erk3$^{-/-}$ and control embryos at E18.5 (Fig. 6*E*). However, IGF-2 levels were significantly lower (27% decrease, $P < 0.01$) in Erk3$^{-/-}$ mutants as compared to wild type littermates, suggesting a defect in the production and/or secretion of IGF-2 in Erk3-deficient mice (Fig. 6*E*).

Discussion

Little is known about the physiological roles of the atypical MAP kinases Erk3 and Erk4. Contrary to other MAP kinases, no ortholog of Erk3 or Erk4 is found in yeast, worms or flies, which precludes the use of these genetically tractable organisms to study their in vivo functions. In vitro studies of Erk3 and Erk4 biology have been hampered by a lack of knowledge of the upstream signals and regulatory inputs that control the expression and/or activity of the kinases. Only a few interacting proteins have been identified for Erk3/Erk4 (20, 21), and MK5 is their only known downstream target (8, 9, 22, 23). In this study, we have used a classical gene targeting approach to explore the physiological function of Erk3. We show that Erk3-deficient mice experience neonatal respiratory morbidity and mortality, and display altered fetal growth potential. Of interest, antenatal glucocorticoid administration rescues the type II pneumocyte maturation defect of Erk3$^{-/-}$ mice but does not impact on neonatal mortality or morbidity. Our results demonstrate that Erk3 is indispensable for neonatal survival and uncover a role of the kinase in fetal growth regulation and pulmonary maturation and function.

A large proportion of *Mapk6*-null mice die immediately after birth from respiratory failure. No cardiac, skeletal or muscular defects were observed in these animals, raising the possibility that the defect was pulmonary in origin. In the mouse, lung development is divided into four stages (24). During the pseudoglandular stage (E9.5–E16.5), branching morphogenesis generates the respiratory tree and the pulmonary vasculature starts to form by vasculogenesis and angiogenesis. At the canalicular stage (E16.5–E17.5), the terminal bronchioles expand to form the respiratory ducts and sacs. The saccular stage (E17.5–PN5) is characterized by thinning of the mesenchyme and differentiation of type I and type II pneumocytes, which are responsible for gas exchange and surfactant production, respectively, to prepare for air breathing. Septation of the saccules that give rise to alveoli starts at postnatal day 5. Histological analysis of lungs taken at different gestation stages indicated that branching morphogenesis is normal in Erk3$^{-/-}$ embryos. However, we observed limited saccular expansion at the end of gestation, which prompted us to investigate the differentiation status of

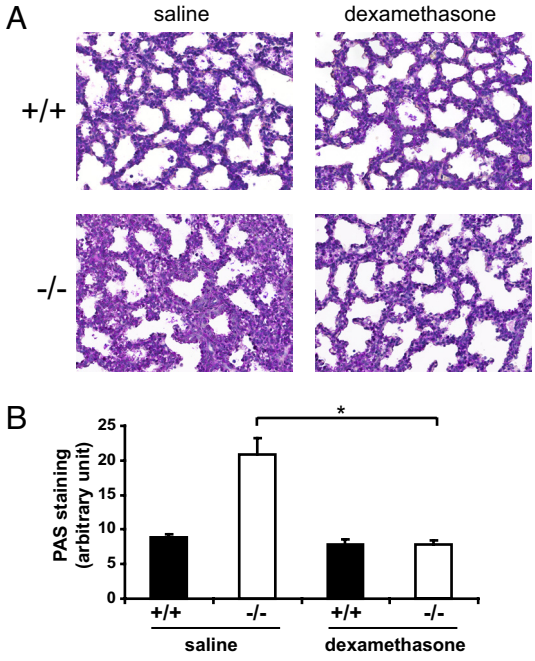

Fig. 5. Antenatal dexamethasone rescues the lung maturation defect of Erk3-deficient mice. (*A*) Pregnant females from Erk3$^{+/-}$ intercrosses were treated with dexamethasone or saline at E16.5 and E17.5 of gestation. Embryos were collected by caesarean section at E18.5 and lung sections were stained with hematoxylin and eosin. Magnification, 40×. (*B*) Quantification of PAS staining in lung sections from E18.5 Erk3$^{+/+}$ and Erk3$^{-/-}$ embryos ($n = 4$–5) treated as in *A*. *, $P < 0.01$.

type I and type II pneumocytes. Abnormal differentiation of type I cells can result in the absence of distal saccular structures, as seen in T1α-deficient mice (25). Here, we show that Erk3$^{-/-}$ lungs inflate apparently normally when fully insufflated, indicating that saccular structures can form in mutant mice. Staining of T1α also demonstrate that type I pneumocyte differentiation is not impaired by *Mapk6* deletion. Immaturity of type II pneumocytes, associated with high glycogen content and decreased surfactant production, leads to respiratory distress and poor neonatal survival (26). We provide evidence that, despite normal SP-C expression, differentiation of type II cells is delayed in Erk3-deficient lungs, as revealed by the persistence of glycogen-rich cells. Importantly, we showed that the pulmonary immaturity phenotype of the mutants can be overcome by antenatal dexamethasone treatment. However, glucocorticoid therapy failed to improve survival of Erk3$^{-/-}$ mice, suggesting that additional physiological alterations contribute to respiratory failure and neonatal lethality. Also, it remains to be established whether the lung defect in *Mapk6* mutant mice is cell-autonomous or a consequence of fetal growth restriction.

In addition to pulmonary functional defects, Erk3-deficient mice display significant (10–15%) growth restriction at birth, which was manifest by E14.5. Consistent with Erk3 signaling modifying fetal growth potential, we found that *Mapk6* gene disruption leads to a 25–40% reduction of visceral organ growth in the lung, heart, and liver that was not attributed to gross morphological abnormalities. The observed decrease in birth weight and organ development is replicative of IUGR conditions as observed in other animal models (27) and human population-based studies (28). In humans, IUGR is defined as birth weight at or below 2 standard deviations for gestational age or approximating $<10^{th}$% of gestational-age adjusted birth weight. Infants with IUGR have not only adverse perinatal outcome, but have a significant risk for diabetes, hypertension and coronary heart

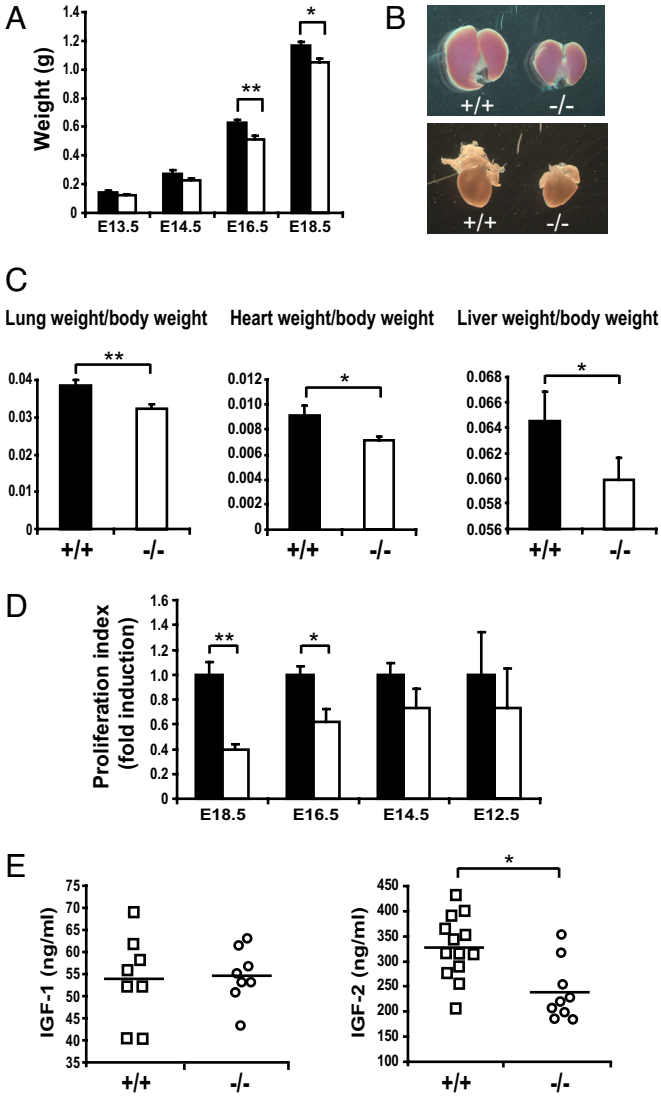

Fig. 6. Growth restriction, attenuated lung cell proliferation, and reduced IGF-2 levels in Erk3-deficient mice. (*A*) Body weight of littermate Erk3$^{+/+}$ (filled bars) and Erk3$^{-/-}$ (open bars) embryos at various developmental stages (n = 6–12). *, $P < 0.05$, **, $P < 0.01$. (*B*) Lungs and heart from wild-type and Erk3$^{-/-}$ E18.5 embryos. (*C*) Ratio of lung, heart and liver weight relative to body weight in wild-type and Erk3$^{-/-}$ E18.5 embryos (n = 8–13). * $P < 0.05$, **, $P <$ 0.01. (*D*) Quantification of cell proliferation assessed by Ki67 immunostaining in lung sections from Erk3$^{+/+}$ (filled bars) and Erk3$^{-/-}$ (open bars) embryos at various developmental stages (n = 3–6). *, $P < 0.05$, **, $P < 0.001$. (*E*) IGF-1 and IGF-2 serum levels in E18.5 wild-type and Erk3$^{-/-}$ embryos (n = 8–13). *, $P < 0.01$.

disease later in life. Moreover, IUGR is associated with long-term neurodevelopmental impairment including reduced neurodevelopmental scores, IQ, and school achievements (29).

IUGR is a complex condition with multiple phenotypic manifestations that may rise from multiple etiologies. From both a clinical and pathophysiological perspective it is advantageous to consider IUGR as a complex disorder, which can be broadly classified as a consequence of maternal/placental, fetal (e.g., genetic aberrations, epigenetic modifications), or secondary to environmental (e.g., fetal infections, teratogens) factors. To gain some insight into the mechanism causing IUGR in Erk3-deficient mice, we measured the circulating levels of the main growth factors controlling intrauterine growth, IGF-1 and IGF-2. Whereas serum IGF-1 levels were unchanged, the levels

of IGF-2 were significantly reduced in Erk3$^{-/-}$ animals. These results suggest a defect in the synthesis and/or secretion of IGF-2 in the absence of Erk3. Genetic studies have clearly established that IGF-2 plays a crucial role in promoting fetal growth. IGF-2-deficient mice are born at 60% the weight of wild type littermates (30), and the decreased growth is apparent as early as E11 (18). IGF-2 is expressed in a wide range of fetal tissues and is found at higher levels in fetal than in adult serum (31). However, besides the study of *Igf2* gene regulation and imprinting, much remains to be known about the complex regulation of fetal IGF-2 expression. Our findings identify Erk3 as a regulator of IGF-2 levels in the mouse. Further characterization of *Mapk6* mutant mice should further our understanding of the genetic and biochemical pathways involved in fetal growth control and pulmonary maturation.

Materials and Methods

For a detailed description of materials and methods, please refer to *SI Text*

Animal Husbandry and Dexamethasone Treatment. Animals were housed under pathogen-free conditions according to the procedures and protocols approved by the Université de Montréal Institutional Animal Care Committee. For breeding, heterozygous males and females in mixed C57BL/6 × 129/Sv background were intercrossed. The presence of a vaginal plug indicated the beginning of gestation (E0.5). Pregnant females were killed at different times by CO_2 euthanasia and embryos were removed by caesarean section. Each embryo was weighted and processed for further analysis. Dexamethasone (Sandoz) or saline control was administered s.c. (0.4 mg/kg) to pregnant females on E16.5 and E17.5.

Quantitative RT-PCR. Total RNA was isolated from E18.5 lung tissue, purified using the RNeasy kit (Qiagen) and reverse transcribed (Applied Biosystems). Real-time analysis of PCR product amplification was performed on the ABI PRISM 7900HT Sequence Detection System (Applied Biosystems).

Immunoblotting Analysis. Mouse embryonic fibroblasts were prepared from E14.5 embryos as described (9). Cell lysis and immunoblot analysis were performed as described (12) using commercial anti-Erk3 (United States Biological; dilution 1:100) or anti-actin (Sigma) antibodies.

Histology and Immunohistochemistry. Tissue sections were stained using conventional hematoxylin/eosin protocol. Lung sections were also stained with PAS. For immunohistochemistry, anti-T1α (Developmental Studies Hybridoma Bank), anti-proSP-C (Chemicon), and anti-Ki67 (Santa Cruz Biotechnology) antibodies were used. For quantitative morphometry, PAS- or Ki67-positive cells, tissue area and saccular airspace were measured with the Image ProPlus software on 10 randomly selected micrographs.

Measurement of IGF Levels. Circulating IGF-1 and IGF-2 levels were measured by ELISA (R&D Systems) according to the manufacturer's instructions.

ACKNOWLEDGMENTS. We thank our colleagues, including Marc K. Saba-El-Leil, Philippe Coulombe, and Elena Sbrana for valuable scientific contributions; D. Lohnes (University of Ottawa) for providing Cre deleter mice; D. Gingras for electron microscopy; C. Charbonneau for microscopic assistance; and Y. Berthiaume and J.A. Whitsett for discussion. B. Turgeon is a recipient of a FRSQ (Fonds de la recherche en santé du Québec) doctoral fellowship. S. Meloche holds the Canada Research Chair in Cellular Signaling. This work was supported by a grant to S. Meloche from the Canadian Institutes for Health Research.

1. Pearson G, et al. (2001) Mitogen-activated protein (MAP) kinase pathways: Regulation and physiological functions. *Endocr Rev* 22:153–183.
2. Coulombe P, Meloche S (2007) Atypical mitogen-activated protein kinases: Structure, regulation and functions. *Biochim Biophys Acta* 1773:1376–1387.
3. Boulton TG, et al. (1991) ERKs: a family of protein-serine/threonine kinases that are activated and tyrosine phosphorylated in response to insulin and NGF. *Cell* 65:663–675.
4. Meloche S, Beatty BG, Pellerin J (1996) Primary structure, expression and chromosomal locus of a human homolog of rat ERK3. *Oncogene* 13:1575–1579.
5. Zhu AX, Zhao Y, Moller DE, Flier JS (1994) Cloning and characterization of p97MAPK, a novel human homolog of rat ERK-3. *Mol Cell Biol* 14:8202–8211.
6. Deleris P, et al. (2008) Activation loop phosphorylation of the atypical MAP kinases ERK3 and ERK4 is required for binding, activation and cytoplasmic relocalization of MK5. *J Cell Physiol* 217:778–788.
7. Cheng M, Boulton TG, Cobb MH (1996) ERK3 is a constitutively nuclear protein kinase. *J Biol Chem* 271:8951–8958.
8. Schumacher S, et al. (2004) Scaffolding by ERK3 regulates MK5 in development. *EMBO J* 23:4770–4779.
9. Seternes OM, et al. (2004) Activation of MK5/PRAK by the atypical MAP kinase ERK3 defines a novel signal transduction pathway. *EMBO J* 23:4780–4791.
10. Turgeon B, Lang BF, Meloche S (2002) The protein kinase ERK3 is encoded by a single functional gene: Genomic analysis of the ERK3 gene family. *Genomics* 80:673–680.
11. Kling DE, et al. (2006) Distribution of ERK1/2 and ERK3 during normal rat fetal lung development. *Anat Embryol (Berl)* 211:139–153.
12. Turgeon B, Saba-El-Leil MK, Meloche S (2000) Cloning and characterization of mouse extracellular-signal-regulated protein kinase 3 as a unique gene product of 100 kDa. *Biochem J* 346(Pt 1):169–175.
13. Coulombe P, Rodier G, Pelletier S, Pellerin J, Meloche S (2003) Rapid turnover of extracellular signal-regulated kinase 3 by the ubiquitin-proteasome pathway defines a novel paradigm of mitogen-activated protein kinase regulation during cellular differentiation. *Mol Cell Biol* 23:4542–4558.
14. Anhe GF, et al. (2006) ERK3 associates with MAP2 and is involved in glucose-induced insulin secretion. *Mol Cell Endocrinol* 251:33–41.
15. Ridsdale R, Post M (2004) Surfactant lipid synthesis and lamellar body formation in glycogen-laden type II cells. *Am J Physiol Lung Cell Mol Physiol* 287:L743–751.
16. Roberts D, Dalziel S (2006) Antenatal corticosteroids for accelerating fetal lung maturation for women at risk of preterm birth. *Cochrane Database Syst Rev* 3:CD004454.
17. Rosenberg A (2008) The IUGR newborn. *Semin Perinatol* 32:219–224.
18. Baker J, Liu JP, Robertson EJ, Efstratiadis A (1993) Role of insulin-like growth factors in embryonic and postnatal growth. *Cell* 75:73–82.
19. Randhawa R, Cohen P (2005) The role of the insulin-like growth factor system in prenatal growth. *Mol Genet Metab* 86:84–90.
20. Hansen CA, Bartek J, Jensen S (2008) A functional link between the human cell cycle-regulatory phosphatase Cdc14A and the atypical mitogen-activated kinase Erk3. *Cell Cycle* 7:325–334.
21. Sun M, et al. (2006) Identification of extracellular signal-regulated kinase 3 as a new interaction partner of cyclin D3. *Biochem Biophys Res Commun* 340:209–214.
22. Aberg E, et al. (2006) Regulation of MAPK-activated protein kinase 5 activity and subcellular localization by the atypical MAPK ERK4/MAPK4. *J Biol Chem* 281:35499–35510.
23. Kant S, et al. (2006) Characterization of the atypical MAPK ERK4 and its activation of the MAPK-activated protein kinase MK5. *J Biol Chem* 281:35511–35519.
24. Maeda Y, Dave V, Whitsett JA (2007) Transcriptional control of lung morphogenesis. *Physiol Rev* 87:219–244.
25. Ramirez MI, et al. (2003) T1alpha, a lung type I cell differentiation gene, is required for normal lung cell proliferation and alveolus formation at birth. *Dev Biol* 256:61–72.
26. Whitsett JA, Weaver TE (2002) Hydrophobic surfactant proteins in lung function and disease. *N Engl J Med* 347:2141–2148.
27. Holemans K, Aerts L, Van Assche FA (2003) Fetal growth restriction and consequences for the offspring in animal models. *J Soc Gynecol Investig* 10:392–399.
28. Lumey LH, Stein AD (1997) Offspring birth weights after maternal intrauterine undernutrition: A comparison within sibships. *Am J Epidemiol* 146:810–819.
29. Leitner Y, et al. (2007) Neurodevelopmental outcome of children with intrauterine growth retardation: a longitudinal, 10-year prospective study. *J Child Neurol* 22:580–587.
30. DeChiara TM, Efstratiadis A, Robertson EJ (1990) A growth-deficiency phenotype in heterozygous mice carrying an insulin-like growth factor II gene disrupted by targeting. *Nature* 345:78–80.
31. Brown AL, et al. (1986) Developmental regulation of insulin-like growth factor II mRNA in different rat tissues. *J Biol Chem* 261:13144–13150.